

Deep Synthesizer Parameter Estimation

Oren Barkan
Tel Aviv University

David Tsiris
Tel Aviv University

ABSTRACT

Sound synthesis is a complex field that requires domain expertise. Manual tuning of synthesizer parameters to match a specific sound can be an exhaustive task, even for experienced sound engineers. In this paper, we propose an automatic method for synthesizer parameters tuning to match a given input sound. The method is based on strided Convolutional Neural Networks and is capable of inferring the synthesizer parameters configuration from the input spectrogram and even from the raw audio. The effectiveness of our method is demonstrated on a subtractive synthesizer with four frequency modulated oscillators, envelope generator and a gater effect. We present extensive quantitative and qualitative results that showcase the superiority of our model over several baselines. Furthermore, we show that the network depth is an important factor that contributes to the prediction accuracy.

1. INTRODUCTION

The art of sound synthesis is a challenging task that mainly reserved to sound designers and engineers [1]. Nowadays, synthesizers play a key role in electronic music production. Typically, music producers are equipped with a set of sound banks per synthesizer. These sound banks are essentially a collection of different configurations (patches) of the synthesizer parameters. Each configuration was carefully tuned by an expert and produces a different type of sound.

During the last decade, the emerge of deep learning advanced the state of the art in various fields such as computer vision [16], speech recognition [17], natural language understanding [18]-[23] and music information retrieval [2]-[4]. Specifically, convolutional neural networks (CNN) were found to be extraordinary learners for genre classification [5]. One of the key properties of CNNs is weight sharing that enables capturing the same patterns in different locations by the application of the same filter function across the signal. This property naturally fits for visual and auditory signals and provides a better generalization performance [6].

In this paper, we investigate the problem of estimating the synthesizer parameter configuration that best reconstructs a source audio signal. We assume the source audio signal is generated from the same synthesizer by a hidden parameters configuration. Therefore, our goal is to reveal the hidden parameters configuration that was used to generate the source signal. This is particularly useful in scenarios where music artists are interested in replicating sounds that were generated by other artists / sound designers using the same synthesizer (assuming no patch is released). Indeed, one of the most frequently asked questions in music production and sound synthesis forums is: What is the recipe for replicating a sound X that was generated by synthesizer Y? An even more general question is: What is the recipe for replicating a sound X using synthesizer Y? while in the former, X is assumed to be synthesized by Y (intra-domain), in the latter, this assumption is no longer valid (cross-domain). This paper focuses on the intra-domain problem and leaves the more general cross-domain problem for future

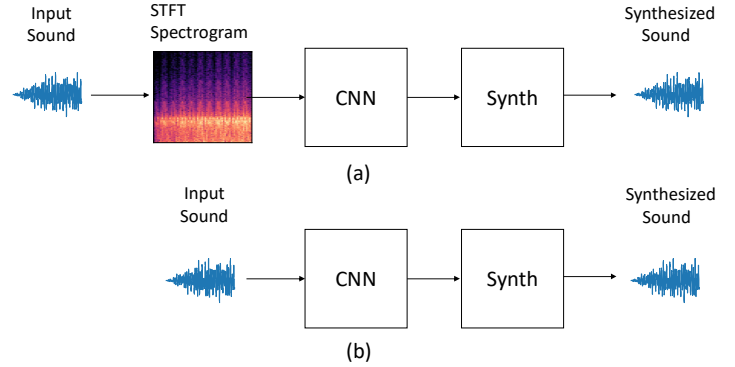


Figure 1. The proposed pipelines. (a) The STFT spectrogram of the input signal is fed into a CNN that predicts the synthesizer parameter configuration. This configuration is then used to produce a sound that is similar to the input sound. (b) End-to-end learning. A CNN predicts the synthesizer parameter configuration directly from the raw audio.

investigation. To this end, we propose to train a 2D strided CNN (with no pooling operations) to predict the synthesizer parameter configuration from the Short Time Fourier Transform (STFT) spectrogram [1] of the input audio signal. Furthermore, we show that a CNN is capable of performing end-to-end learning directly from the raw audio to the synthesizer parameters domain, successfully. This is done by adding several convolutional layers that are designed to learn an alternative representation for the STFT spectrogram.

The proposed pipelines are depicted in Figure 1. In Fig.1 (a), an input audio signal is transformed to a STFT spectrogram matrix, which is then fed to a CNN. The CNN analyzes the spectrogram and predicts a parameter configuration. Finally, the synthesizer is configured according to the predicted parameters values and synthesizes the output audio signal. In Fig. (b), a CNN performs end-to-end learning and predicts the parameters configuration directly from the raw audio. In addition, we compare the performance of these models against two other types of fully connected (FC) neural network models: the first type is a FC network that receives a Bag of Words (BoW) representation of the spectrogram as input. The second type is a FC network that receives a set of complex hand crafted features [10] that are designed to capture spectral properties and temporal variations in the signal.

The audio signals that are used for training and testing the models are generated by synthesizer parameter configurations that are randomly sampled, i.e. for each synthesizer parameter, we define an effective range of valid values and sample the parameter value from this range, uniformly. Hence, each configuration in the dataset is obtained by a set of (parameter, sampled value) pairs.

We present a comprehensive investigation of various network architectures and demonstrate the effectiveness of the proposed

method in a series of quantitative and qualitative experiments. Our findings show that the network depth is an important factor which contributes to the prediction accuracy and a spectrogram based CNN of a sufficient depth outperforms its end-to-end counterpart, while both CNN variants significantly outperform Fully Connected networks.

2. RELATED WORK

The problem of synthesizer parameter estimation has been studied in the literature. Several attempts has been made to apply traditional machine learning techniques to physical modeling of musical instruments such as bowed and plucked strings [7]–[9]. However, in this work, we focus on subtractive synthesis with frequency modulation (FM) [1] which is the most common synthesis method in electronic music production and enables the creation of extremely diversified sounds. This is in contrast to physical modeling synthesis that is mainly used for creating real-sounding instruments, as it is programmed to make characteristic distinctions between various aspects of the instrument being created and is rarely used by music producers.

Itoyama and Okuno [10] proposed to apply a multiple linear regression from a set of handcrafted features to the synthesizer parameter domain. Our approach, differs from [10] by two main aspects: first, we solve a classification task rather than a regression. Second, we propose deep CNN architectures with non-linear gates. These networks have enough capacity to learn complex filters (weights) that are capable of capturing important patterns and yet generalize well. This eliminates the need for handcrafted features and enables the use of STFT spectrogram or raw audio as input without further manipulations. We validate this claim, empirically, by comparing the CNN models to linear and non-linear FC models that use the hand crafted features from [10].

3. SYNTHESIZER ARCHITECTURE AND PARAMETERS

This section describes the synthesizer architecture that is used in this work. The synthesizer is implemented using JSyn [11], an open source library that provides audio synthesis API for Java. The reason we use JSyn is twofold: most of commercial synthesizers usually do not provide an API for generating sounds programmatically. This makes the dataset generation process impractical (in this work, we use a dataset that contains 200K instances). Second, commercial synthesizers are not open source and quite expensive. Therefore, we avoid of using these synthesizers in order to make our research reproducible.

In similar to the majority of modern synthesizers, we employ subtractive and FM synthesis [1]. The synthesizer architecture is a cascade of four components and is depicted in Fig. 2. The first component is a set of oscillators, each produces a different waveform type: sine, saw, square and triangle [1]. All oscillators are frequency modulated by a sinusoidal waveform. An oscillator function is defined as

$$y_w(f, v, A, B) = Ax_w(2\pi ft + B\sin(2\pi vt)) \quad (1)$$

where f, v, A, B are the carrier frequency, modulation frequency, carrier amplitude and modulation amplitude, respectively, while $w \in W$ is the waveform type with $W = \{\sin, \text{saw}, \text{tri}, \text{sqr}\}$ and

$$\begin{aligned} x_{\sin}(a) &= \sin(a), \\ x_{\text{saw}}(a) &= 2^{-1} - \pi^{-1} \sum_{n=1}^{\infty} n^{-1} (-1)^n \sin(na), \end{aligned}$$

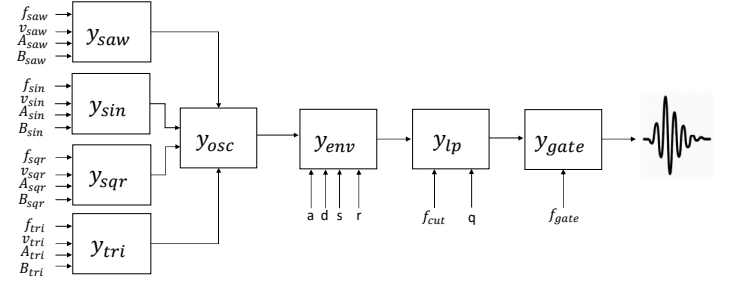


Figure 2. The subtractive synthesizer used in this work. The synthesizer has four frequency modulated oscillators, ADSR envelope generator, low-pass filter and gater effect. See Section 3 for details.

$$\begin{aligned} x_{tri}(a) &= 2^{-1} - \pi^{-1} \sum_{n=1}^{\infty} n^{-2} (-1)^n \sin(na), \\ x_{sqr}(a) &= \text{sgn}(\sin(a)). \end{aligned}$$

Note that each oscillator y_w is associated with its **own** set of f_w, v_w, A_w, B_w parameters. Finally, the outputs from all oscillators are summed to $y_{osc} = \sum_{w \in W} y_w$. Therefore, the total number of parameters in the y_{osc} component is 16.

The function y_w from Eq. (1) is a special case of a general family of frequency modulated functions of order $n \in \mathbb{N}$:

$$y(\Psi, \Phi, \Omega) = \psi_0 x_{\phi_0} (2\pi \int_0^t \gamma_0(t_0) dt_0), \quad \text{with}$$

$$\gamma_0(t_0) = \omega_0 + \psi_1 x_{\phi_1} (2\pi \int_0^{t_0} \gamma_1(t_1) dt_1), \dots, \gamma_n(t_n) = \omega_n$$

where $\Psi = (\psi_i)_{i=0}^n$, $\Phi = (\phi_i)_{i=0}^n$, $\Omega = (\omega_i)_{i=0}^n$ are the amplitudes, waveforms and frequencies series and it holds that $\forall i: \phi_i \in \Lambda$, where Λ is a set of periodic functions symbols, i.e. the waveform symbols set. In this work, we focus on frequency modulated functions y of order 1 with $\phi_0 \in W$ and $\phi_1 = \sin$ as defined in Eq. (1).

The second component is the *Attack Decay Sustain Release* (ADSR) envelope generator [1] $y_{env}(x, a, d, s, r)$. This component controls the amplitude of the input x at any point in the signal duration. The contour of the ADSR envelope is specified using four parameters: a (*Attack*) is the time taken for initial run-up of level from zero to peak, beginning when the key is first pressed. d (*Decay*) is the time taken for the subsequent run down from the attack level to the designated sustain level. s (*Sustain*) is the level during the main sequence of sound's duration, until the key is released. r (*Release*) is the time taken for the level to decay from the sustain level to zero after the key is released.

The third component is the filter $y_{lp}(x, f_{cut}, q)$ that consists of a low-pass filter together with a resonance [1]. Setting a cutoff frequency f_{cut} ensures that all frequencies above f_{cut} are cut. The resonance parameter q determines a narrow band of frequencies near f_{cut} that are amplified.

The last component in the chain is the gater effect that controls the rate of the amplitude. The gater is a Low Frequency Oscillator (LFO) that performs amplitude modulation to the input, according to a sine waveform with a frequency f_{gate} :

$$y_{gate}(x, f) = ((1 + x_{sqr}(2\pi f_{gate}t))/2)x(t)$$

Figure 2 illustrates the synthesizer function that has 23 parameters and is given by $y_{gate} * y_{lp} * y_{env} * y_{osc}$, where $*$ stands for the function composition.

4. DATASET GENERATION

The synthesizer described in Section 3 is used for generating the dataset. For each synthesizer parameter, we perform a quantization to a set of 16 levels and treat each level as a different class. Hence, we formulate the parameter estimation task as a classification problem rather than a regression - our model aims at predicting for each parameter in the synthesizer the correct class (value). This choice is made in order to use the binary cross entropy loss [6] that is easier to optimize than the L2 loss and is on par with previous works [12]. Moreover, the classification formulation allows us to use several measures (Section 6) that enable better quantification and understanding of the parameter estimation accuracy.

The range of the carrier frequency f is quantized according to $f = 2^{n/12} \times 440\text{Hz}$ with $n \in \{0..15\}$. This produces frequencies that correspond to the 16 consecutive musical notes $A_4 - C_6$. The rest of the synthesizer parameters ranges are quantized evenly to 16 classes according to the following ranges: the amplitudes and ADSR envelope parameters A_w, a, d, s, r are in $[0.001, 1]$, the modulation amplitudes B_w are in $[0, 1500]$ (where $B_w = 0$ means no frequency modulation), the modulation frequency, gating frequency, cutoff frequency and resonance $v_w, f_{gate}, f_{cut}, q$ are in $[1, 30]$, $[0.5, 30]$, $[200, 4000]$, $[0.01, 10]$, respectively. For each parameter, the first and last classes correspond to its range limits. All ranges and sampling patterns are set in order to avoid sound generation that is indistinguishable by human hearing and better match a linear perception.

The dataset consists of (g, h) pairs, where h is the label vector that corresponds to a specific synthesizer parameter configuration and g is the raw audio signal produced by the configuration that is associated with h . The generation process of a single pair (g, h) works as follows: for each synthesizer parameter j , we sample a class from a uniform categorical random variable $u \in \{0, \dots, 15\}$ and create an one-hot encoding vector $h_i \in \{0, 1\}^{16}$ for the sampled class. Then, we concatenate all the vectors to a single supervector $h = [h_1, \dots, h_{23}] \in \{0, 1\}^{368}$ that contains the one-hot encoding for each parameter in the corresponding section in h . Then, the synthesizer parameters are configured according to values that correspond to the sampled classes in h and an output audio signal in a duration of 1 second with a sampling rate of 16384Hz $g \in [-1, 1]^{16384}$ is produced.

Recall that we consider two types of CNN architectures: an end-to-end (Fig. 1(b)) and a spectrogram based (Fig. 1(a)), where the latter requires further transformation over g . Therefore, the STFT spectrogram of g is computed with half overlapping windows of size 512 to produce a matrix $S \in \mathbb{R}^{257 \times 64}$. This matrix contains 64 vectors in size of 257 that correspond to the absolute of the Fourier Transforms (FT) of 64 consecutive time windows. Note that the application of FT produces 512 complex values. However, we discard half of them since the FT of real signals is conjugate symmetric. This process is repeated 200k times to produce two datasets: $D_{E2E} = \{(g_k, h_k)\}$ and $D_{STFT} = \{(S_k, h_k)\}$ that are used for training the end-to-end and spectrogram based CNNs, respectively.

5. MODELS AND METHODOLOGY

In this section, we describe the CNN components from the two different pipelines that appear in Fig. 1. The goal of these components is to learn a function from the STFT / raw audio domains to the synthesizer parameter domain. To this end, we propose to train CNNs using the datasets described in Section 4 to predict the correct parameter classes (values) from the STFT matrix / raw audio. As a baseline, we further consider the replacement of the CNNs with Fully Connected (FC) neural networks. All models

share the common property of having an output layers in size of 368 with sigmoid activations (to match h 's dimension). Note that an alternative is to apply 23 separated softmax activations that are fed into 23 categorical cross entropy loss functions (for each synthesizer parameter in separate) and compute the final loss as the summation of the 23 loss functions. While this alternative approach seems more natural, in our initial experiments, it performs slightly worse. Therefore, we ended up with using sigmoid activations with binary cross entropy loss.

In order to isolate the effect of network depth, we restrict all networks to have the same number of trainable parameters, regardless of their depth. This ensures that better results, when obtained using a deeper model, are indeed due to the increase in depth. Yet, we did conduct an initial investigation to find a saturation point - a point in which a further increase in number of trainable parameters (model capacity) results in a marginal contribution to the model accuracy. In what follows, we describe the models used for evaluation.

5.1 Fully Connected Neural Networks

A FC neural network is a feed forward network in which each neuron is connected to all neurons in the previous layer [6]. This type of networks expect to have 1D input (vector). Since the training instances are STFT matrices / raw audio signals, the trivial choice is to feed the FC network with the raw audio vectors / flattened STFT matrices. However, in our initial experiments both approaches produced poor results. This is due to the fact that both flattened STFT matrices and raw signals are not time invariant and of extremely high dimension ($\sim 16K$).

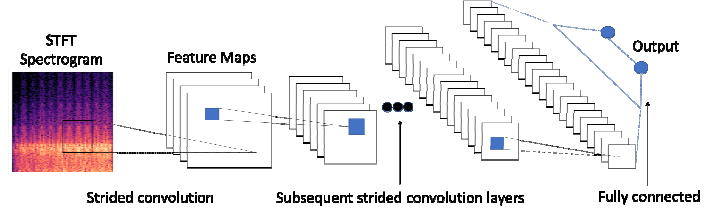
In order to alleviate this problem, we propose to use two different types of input representation to the FC models: the first type is based on the STFT matrix. Specifically, we first apply PCA to the STFT frequency axis to produce a STFT-PCA matrix with a reduced frequency-PCA dimension of 64 (while retaining 97% of the variance). Then, we learn a Bag of Words (BoW) [13] representation of the STFT-PCA matrices. To this end, we Vector Quantize [13] the STFT matrices using K-means [13] with $K = 1000$ and assign each row vector in the STFT-PCA matrix to its closest centroid. This produces a count vector in size 1000, in which the i -th entry counts the number of vectors that were assigned to i -th centroid. Finally, we convert the counts to probabilities by normalizing each count vector by the sum of its entries. This results in a time invariant representation of a reduced dimensionality.

We consider four different FC model architectures that use the BoW representation as input: the first model has a single hidden layer with linear activations and is dubbed FC Linear (note that in this work, we define the number of layers in a network, as the number of hidden layers in between the input and output layers). Hence, FC Linear is equivalent to a logistic regression model with a hidden layer. The three other models are dubbed FC1, FC2 and FC3 and have 1, 2 and 3 hidden layers with ReLU [6] activations, respectively. We observed that further increase in network depth to more than 3 layers did not contribute to improved performance.

The second type of representation input that we consider is a set of complex hand crafted features [10] that are computed from the raw audio signal. These features are designed to capture spectral and temporal properties of the signal. In what follows, we briefly describe the feature extraction process. First are computed the energy levels of the signal in various bands, zero crossing rate, spectral width, spectral centroid, spectral rolloff, spectral flux, spectral peak, spectral peak and valley, spectral contrast, Mel-Frequency cepstrum Coefficients (MFCCs) and timbre of the harmonic components. These features are computed framewise and produces a 32 dimensional feature vector per frame. In order to

Table 1. FC and HC models architectures (see Section 5.1)

FC and HC Architectures					
FC Linear	FC1	FC2	FC3	HC	HC3
1 Layer	1 Layer	2 Layers	3 Layers	1 Layer	3 Layers
FC input: BoW vector in size of 1000 for FC models. HC input: Vector in size of 1000 [10]					
FC-869	FC-868	FC-603	FC-560	FC-869	FC-560
Drop-0.2	Drop-0.3	Drop-0.1	FC-500	Drop-0.2	FC-500
		FC-602	Drop-0.2		Drop-0.2
		Drop-0.3	FC-400		FC-400
			Drop-0.4		Drop-0.4
FC-368(sigmoid)					

**Figure 3.** A generic illustration of the spectrogram based 2D strided CNN architecture. See Section 5.2 for details.**Table 2.** CNN models architectures (see Section 5.2 for details)

Conv Architectures							
Conv 1	Conv2	Conv3	Conv4	Conv5	Conv6	Conv6XL	ConvE2E
2 Layers	3 Layers	4 Layers	5 Layers	6 Layers	7 Layers	7 Layers	11 Layers
Input (64 X 257 STFT Spectrogram)							Input (16384 raw audio)
C(38,13,26,13,26)	C(35,6,7,5,6)	C(32,4,5,3,4)	C(32,3,4,2,3)	C(32,3,3,2,2)	C(32,3,3,2,2)	C(64,3,3,2,2)	C(96,1,64,1,4)
	C(87,6,9,5,8)	C(98,4,6,3,5)	C(65,3,4,2,3)	C(98,3,3,2,2)	C(71,3,3,2,2)	C(128,3,3,2,2)	C(96,1,32,1,4)
		C(128,4,6,3,5)	C(105,3,4,2,3)	C(128,3,4,2,3)	C(128,3,4,2,3)	C(128,3,4,2,3)	C(128,1,16,1,4)
			C(128,4,5,3,4)	C(128,3,5,2,4)	C(128,3,3,2,2)	C(128,3,3,2,2)	C(257,1,8,1,4)
				C(128,3,3,2,2)	C(128,3,3,2,2)	C(256,3,3,2,2)	C(32,3,3,2,2)
					C(128,3,3,1,2)	C(256,3,3,1,2)	C(71,3,3,2,2)
							C(128,3,4,2,3)
							C(128,3,3,2,2)
							C(128,3,3,2,2)
							C(128,3,3,1,2)
FC-512							
FC-368(sigmoid)							

capture temporal variation, this feature vector is further extended (by concatenation) with several types of time derivatives that produced an extended feature vector of dimension 224. Then, all framewise feature vectors are accumulated along the time axis via the computation of the following statistics: summation, mean, variance, skewness, minimum, maximum, median, 10th and 90th percentiles, where the last five are computed with their positions in time to capture temporal structure. In addition, the bottom 10 coefficients of the discrete cosine transform are computed. This procedure is repeatedly applied for 25 different segments of the signal in order to characterize the signal in different temporal regions. Finally, all segment-wise feature vectors are concatenated to produced a feature supervector in dimension of 319,200 that is reduced to dimension of 1000 by the application of PCA. The reader is referred to Section 2 in [10] for a detailed description of the exact feature extraction process.

We consider two different FC model architectures that use the input representation from [10]. The first is a linear FC model that is equivalent to the one from [10], but uses a classification output layer instead of regression (In our initial experiments, we tested regression models and observed they perform worse than classification models). We dub this model ‘HC’ (hand crafted). In addition, we investigated whether a nonlinear FC model can benefit from using the features from [10]. We found that a FC network with 3 ReLU activated layers and a dropout in between achieves the largest improvement over HC [10], while further increase in depth or number of trainable parameters results in overfitting with worse values of validation loss. We dub this model ‘HC3’. Note that HC3 is an improvement we suggest, in order to showcase the potential

gain that can be achieved by using the features from [10] with deep neural networks.

For all models in this section, a dropout [6] is applied after each hidden layer in order to avoid a severe overfitting. The exact architectures, for each FC model is detailed in Table 1, where FC-k stands for a FC layer with output size of k and Drop-p stands for a dropout that is applied to the input of the next layer with a probability p. All FC models have ~1.2M trainable parameters.

5.2 Strided Convolutional Neural Networks

A CNN [6] is a special type of neural network that employs weight sharing. This property enables the reuse of the same set of weights in all positions in the input. The CNN weights act as local filters that are being convolved with the input. This results in a network with a fewer neuron connections than in FC networks (in which every neuron is connected to all neurons in the previous layer). In addition, Max-Pooling (MP) [6] is often applied to downsample the input in between layers.

In this work, we use 2D CNNs as these were found to improve on the state of the art in music and audio related tasks [5]. Different from [5], we do not perform any type of pooling operations. Instead, we use strided convolutions layers [6], as we found this approach to significantly outperform the traditional setup of ordinary convolutions layers with pooling in between.

Two types of CNNs are considered: the first type is a spectrogram based CNN that receives the STFT matrix as input. This network learns filters that analyze the input in both frequency

Table 3. MPR values for each combination of model and parameter. Last line presents the mean MPR across all parameters per model.

Parameter	FC Linear	FC1	FC2	FC3	Conv1	Conv2	Conv3	Conv4	Conv5	Conv6	Conv6XL	ConvE2E	HC	HC3
a	59.34	61.46	61.59	61.23	69.15	69.28	69.67	69.91	70.66	71.28	70.85	84.38	75.74	83.59
d	53.23	52.99	53.04	53.2	53.3	53.7	53.69	54.05	53.64	53.53	53.53	53.98	53.87	53.12
s	53.09	53.48	53.2	53.45	52.76	53.69	53.38	53.43	53.55	53.32	53.55	54.01	53.33	53.09
r	59.49	61.76	62.25	61.99	81.32	83.79	85.88	88.04	88.43	90.47	90.23	88.52	76.4	88.46
f_{gate}	54.49	55.48	55.89	55.49	81.03	96.02	96.6	97.66	97.85	97.54	97.88	92.81	91.99	94.02
f_{cut}	91.27	92.83	93.05	92.9	98.64	99.07	99.48	99.59	99.64	99.71	99.68	98.5	96.76	99.27
q	79.84	82.22	82.59	82.38	90.46	92.55	94.39	95.34	96.1	96.46	96.62	93.3	85.25	94.55
A_{saw}	65.41	66.99	67.96	68.09	68.05	72.05	74.02	74.95	76.36	76.5	77.12	69.54	66.54	75.66
B_{saw}	82.58	83.25	82.8	82.46	81.03	83.75	84.04	85.01	85.4	85.7	85.73	79.76	81.97	81.85
v_{saw}	55.31	56.04	56.51	56.28	59.62	66.56	67.12	67.98	67.33	67.18	66.79	65.58	64.46	63.75
f_{saw}	72.54	74.02	73.36	72.71	70.31	77.74	78.27	79.93	79.65	79.86	80.16	73.85	73.72	74.93
A_{sin}	54.56	55.52	56.05	55.91	59.73	63.33	65.3	65.84	66.45	66.8	67.28	64.7	60.16	65.79
B_{sin}	80.43	81.03	81.33	80.74	82.06	84.3	84.43	85.67	85.95	86.42	86.5	81.49	83.72	83.89
v_{sin}	54.24	54.87	54.97	54.48	60.91	67.88	68.18	68.73	68.53	68.38	68.02	67.45	65.4	64.4
f_{sin}	60.19	62.09	62.12	61.15	64.73	79.08	79.5	80	80.62	80.55	80.41	75.33	73.26	75.23
A_{sqr}	65.17	67.22	68.13	68.07	65.51	71.51	73.04	74.46	75.31	75.65	76.46	72.08	65.88	75.69
B_{sqr}	85.98	87.61	87.6	87.34	85.65	88.54	89.01	89.99	90.51	90.77	90.85	83.89	86.69	87.98
v_{sqr}	57.42	59.31	59.8	59.76	63.89	69.47	69.94	70.25	69.99	69.68	69.55	68.91	68.39	67.82
f_{sqr}	76.29	78.76	78.44	77.79	75.02	83.2	83.88	84.8	85.39	85.79	86.27	78.38	78.46	81.62
A_{tri}	54.15	54.93	55.39	55.38	58.53	61.78	63.1	63.99	64.76	64.7	65.41	61.73	57.55	61.61
B_{tri}	79.8	80.41	80.48	79.97	81.15	82.43	82.53	83.76	84.27	84.45	84.27	80.41	81.99	82.15
v_{tri}	54.28	54.49	54.48	54.3	59.43	66.55	66.94	67.49	67.25	66.91	66.61	66.8	63.49	63.07
f_{tri}	59.53	60.96	61.12	59.52	63.61	76.66	77.3	78.13	78.48	78.03	77.9	73.62	69.94	72.71
Mean MPR	65.59	66.85	67.05	66.72	70.69	75.78	76.51	77.35	77.66	77.81	77.9	76.17	72.8	75.8

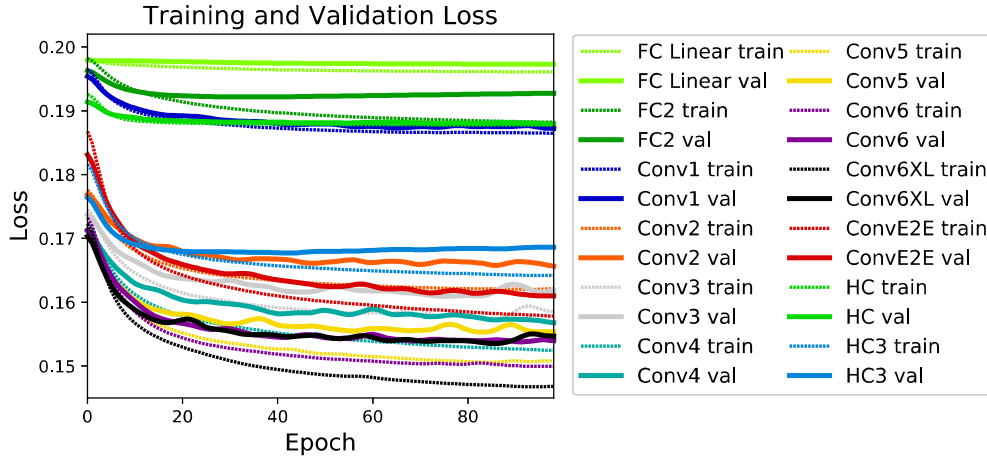


Figure 4. Training and validation loss graphs for all models.

and time axes, simultaneously and is illustrated in Fig. 3. We investigate seven different spectrogram based CNNs. The first six models share the same number of 1.2M trainable parameters, but vary by network depth. These models are dubbed Conv1, ..., Conv6 and have 1, ..., 6 2D strided convolutional layers, respectively. The seventh CNN is dubbed Conv6XL and has 6 strided convolutional layers, but 2.3M trainable parameters. The reason we further include Conv6XL in the evaluation is to check whether increasing the model capacity, in terms of number of trainable parameters, further contributes to the prediction accuracy.

The second type of CNN is an end-to-end CNN that receives the raw audio signal as input. This network is dubbed ConvE2E and further aims at learning a set of filters that produce a transformation on the raw audio, which is an **alternative** to the STFT spectrogram. Hence, the first four layers in the ConvE2E model are dedicated to transform the 16K dimensional input signal to a matrix in the exact

same size of the STFT matrix (64x257). These four layers are 1D strided convolutional layers that operates on the time axis only. This is followed by additional six 2D strided convolutional layers that are identical to those of Conv6 model. Due to the extra four layers, ConvE2E has 1.9M trainable parameters. Finally, all CNN models have an additional FC hidden layer in between the last convolutional layer and the output layer.

The exact models architectures are detailed in Table 2, where $C(F, K1, K2, S1, S2)$ stands for a ReLU activated 2D strided convolutional layer with F filters in size of $(K1, K2)$ and strides $(S1, S2)$. In the case of ConvE2E, the first four layers degenerates to 1D strided convolutions by setting both $K1$ and $S1$ to 1. Finally, it is worth noting that no dropout is applied in the CNNs, since we found that CNNs less tend to overfitting.

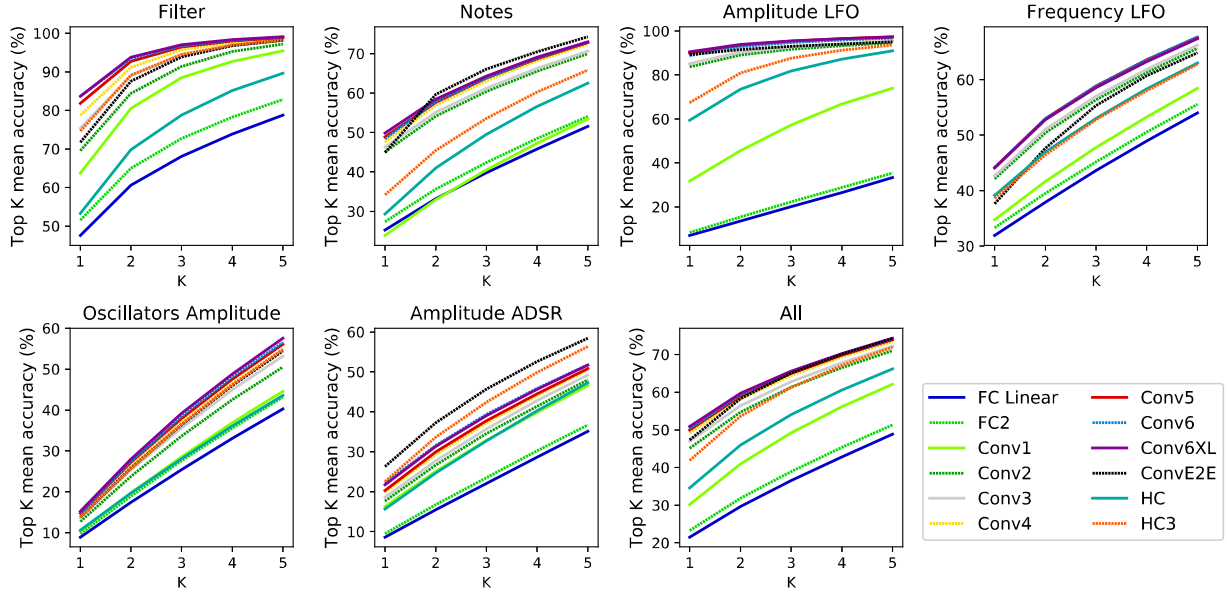


Figure 5. Top-k mean accuracy graphs for various combinations of models and parameter groups. See Section 6.1.2 for details.

6. EXPERIMENTAL SETUP AND RESULTS

In this section, we describe the experimental setup, evaluation measures and present quantitative and qualitative results. The reported results are obtained using 10 fold cross validation on the datasets that are described in Section 4.

The evaluated models are specified in Tables 1 and 2. All models are optimized w.r.t. the binary cross entropy loss [6] using ADAM [14] optimizer with mini batch size of 16 for 100 epochs.

6.1 Quantitative Results

The training and validation loss per model are displayed in Figure 4. We can see that most of the CNN models obtain significantly lower validation loss values than their FC and HC counterparts. Specifically, Conv6XL and Conv6 perform the best and on par with each other. Therefore, we conclude that increasing the number of trainable parameters from 1.2M to 2.3M has a negligible effect for CNNs of a sufficient depth. The largest decrease in loss is obtained when moving from Conv1 to Conv2 and then from Conv2 to Conv3. We believe that this is since Conv1 and Conv2 uses strides values that results in too aggressive subsampling. The ConvE2E model significantly underperforms Conv4, Conv5, Conv6 and Conv6XL, but is on par with Conv3 and outperforms all FC and HC models. Hence, we conclude that the STFT spectrogram contains further crucial information that ConvE2E fails to extract from the raw audio. On the other hand, ConvE2E manages to learn filters that are better than the complex hand crafted features from [10], even when combined with a deep FC network (HC3).

In the case of FC models, FC2 performs the best, but still much worse than all CNNs. FC Linear performs the worst among all models. Note that we omit the loss graphs of FC1 and FC3 for better clarity as these almost completely overlap with FC2. Examining the performance of the HC models, we observe the following trends: HC which is a linear model outperform all non-linear FC models and is on par with Conv1. This can be explained by the fact that HC uses hand crafted features that are far more complex than the STFT spectrogram and its BoW representation. HC3 significantly

outperform HC and Conv1. Yet, HC3 is still outperformed by most of the Conv models including ConvE2E.

Figure 4 further shows that network depth plays an important factor: the deeper the network the better it manages to learn (recall that all models have the same number of trainable parameters except for Conv6XL and ConvE2E). Specifically, we observe that a large reduction in loss is obtained by moving from HC to HC3, despite the fact both models have the same number of trainable parameters. This is another evidence for the importance of network depth which results in additional nonlinear transformations. However, the contribution from depth becomes marginal, when using more than 5, 2 and 3 layers for CNN, FC and HC models, respectively.

In terms of generalization, FC1, FC2, FC3 and HC3 start overfitting after ~20 epochs. We tried to alleviate this problem by increasing the dropout values and applying L2 regularization, but this resulted in higher values of validation loss. In the case of CNN models, no overfitting is observed, despite the fact that no regularization is applied. We believe that this is due to nature of CNNs that enables weight sharing and the fact that the signals we deal with originate in a family of periodic functions that exhibit stationarity (Eq. (1)), excluding the effect of the ADSR envelope.

Although the models are optimized w.r.t. the binary cross entropy loss, our goal is to measure the reconstruction quality in terms of human hearing. As we are not aware of any quantitative measure that correlates well with human hearing, we propose several additional measures to evaluate the models performance in multiple resolutions: accuracy per parameter, accuracy per group of parameters and reconstruction quality in both time and frequency domains.

6.1.1 Mean Percentile Rank (MPR) based Evaluation

The first measure is the Mean Percentile Rank (MPR) which is computed per synthesizer parameter. Formally, we denote by r_i the ranked position of the correct class, when measured against the other classes based on prediction scores output by the model. In our case, we have 16 classes. Hence, the MPR measure is computed according to $MPR = 100 \times (1 - \frac{1}{|\mathcal{T}|} \sum_{i \in \mathcal{T}} \frac{r_i}{15})$ where \mathcal{T} is the number of test instances. Note that $0 \leq MPR \leq 100$, where

Table 4. Reconstruction quality for the evaluated models in time and frequency domains. ρ values are x100. See Section 6.1.3 for details.

Measure/Model	Conv6XL	Conv6	Conv5	Conv4	ConvE2E	HC3	HC [10]	FC2	FC Linear
ρ mean (STFT)	92.04	91.38	91.09	90.97	88.33	88.04	84.62	77.22	75.24
ρ median (STFT)	95.61	95.39	95.1	94.99	93.41	92.59	88.53	82.32	80.83
ρ mean (FT)	76.13	74.28	73.46	73.29	71.36	64.39	59.68	58.18	54.74
ρ median (FT)	90.22	88	87.4	86.29	80.61	68.07	59.73	57.19	51.15
ρ mean (time)	63.19	61.15	60.39	59.65	57.26	50.31	45.54	41.98	38.43
ρ median (time)	86.11	82.92	82.57	81.08	73.81	54.83	40.94	38.81	32.1
F_Δ mean (STFT)	708.94	740.32	757.69	765.55	904.12	918.78	1117.53	1336.7	1427.03
F_Δ median (STFT)	679.36	704.99	726.87	743.97	884.96	916.52	1084.59	1267.87	1328.79

$MPR = 100$ is the optimal value and $MPR = 50$ can be achieved by random predictions.

Table 3 presents the obtained MPR values for each combination of model and synthesizer parameter. We see that the same trends that exist in Figure 4 also exist in Table 3. CNNs produce higher MPR values than FC models in most cases. An exception is the MPR values obtained for the decay and sustain parameters d, s . This can be explained by the fact that these parameters have a negligible influence on the signal amplitude comparing to the attack and release. Moreover, the ADSR envelope determines the change in amplitude over time and has a small effect over the sound timbre. Therefore, we find that bad MPR values for d, s does not mean bad signal reconstruction in terms of human hearing. An interesting observation is that ConvE2E, HC and HC3 models produce significantly better MPR scores for the attack parameter a . This implies that ConvE2E dedicates filters for capturing volume transients that are also captured by the temporal feature extraction scheme of [10]. In addition, we observe that for the modulation frequency v_w , the best MPR values are obtained by the Conv4 across all waveforms W , but by a small margin over Conv5 / Conv6. The last row in Table 3 contains the mean of MPR values per model across all synthesizer parameters. We see that Conv6XL produces the best value, where the second best value is obtained by Conv6. ConvE2E is on par with Conv3 and slightly better than HC3. Finally, HC models significantly outperform all FC models.

6.1.2 Top-k Mean Accuracy based Evaluation

The second measure is the top-k mean accuracy. For a given test example, the top-k accuracy function outputs 1 if the correct class rank is among the top k predicted classes by the model and 0 otherwise. The top-k mean accuracy is obtained by computing the top-k accuracy for each test example and then taking the mean across all examples. In the same manner as done in the MPR analysis, we compute the top-k mean accuracy per synthesizer parameter for $k = 1, \dots, 5$. Then, we group the synthesizer parameters according to the following functionality groups: Filter group that contains the parameter f_{cut}, q . Notes, Amplitude LFO, Frequency LFO and Oscillators Amplitude groups that contain the parameters f_w, B_w, v_w, A_w for all w , respectively. The last two groups are the Amplitude ADSR group that contains the parameters a, d, s, r and the All group that contains all the synthesizer parameters.

For each combination of model and parameter group we compute the mean of the top-k mean accuracy across all parameters in that group and for all k values. The reason we divide the parameters into different groups is in order to inspect the models performance w.r.t. each functional in the synthesizer. Figure 5 presents top-k mean accuracy as a function of k for each combination of parameter group and model. We can see that the results correlate well with Table 3. The best accuracy values are obtained for the Filter and Amplitude LFO groups, where the margin between the CNN and FC models is the largest. Furthermore, in all graphs the CNNs significantly outperform the FC models. Finally, we observe that

for the Amplitude ADSR parameter group, ConvE2E produces the best accuracy graph followed by HC3 as the second best. This is directly related to the ability of these models to predict the attack parameter significantly better than the other models. An interesting pattern is further observed in the Notes graph: while ConvE2E significantly underperforms Conv4 – Conv6XL for $k = 1$, It becomes the champion for $k > 1$. This means that ConvE2E manages to infer a better ranking of musical notes when considering the predictions beyond the one on the top.

6.1.3. Reconstruction Quality in Time and Frequency Domains

In the last two sections, we evaluated the parameter estimation accuracy obtained by the models. In this section, we investigate how well the pipeline as a whole reconstructs the input signals using the different models. The evaluation is conducted both time and frequency domains and focuses on a subset of the models that performed the best among each model type (Linear FC, non-linear FCs, HCs and CNNs)

The first two evaluations are performed in the STFT domain. Specifically, we compute for each signal x_i in the test set its STFT representation S_i . Then, S_i is fed to the model to produce the synthesizer parameter configuration which is then used to synthesize an output signal x_o using the synthesizer. Finally, we compute the STFT representation S_o of x_o . Note that in the case of ConvE2E and HC models x_i is fed as input (HC models further require the preprocessing of [10] on x_i)

We propose two measures to quantify the reconstruction quality in the STFT domain. The first one is the Frobenius norm of the difference between S_i and S_o . To this end, we denote $F_\Delta = \sqrt{\text{Tr}(UU^T)}$ with $U = S_i - S_o$. The lower F_Δ the better the reconstruction quality. The second measure is the Pearson Correlation Coefficient (PCC) $\rho(x, y) = \frac{\text{cov}(x, y)}{\sigma_x \sigma_y}$. Since ρ is defined over vectors rather than matrices, we flatten S_i and S_o to vectors by performing rows concatenation and then compute their PCC value.

The third evaluation is designed to quantify the reconstruction quality in the Fourier domain. To this end, denote the FFT representation of x_i and x_o as we compute the PCC over the absolute of the Fourier Transforms (FT) of x_i and x_o . Different from the STFT, which provides the frequency information per short time frames, the FT provides a global representation that aggregates the frequency information from the entire signal. Lastly, the fourth evaluation is designed to quantify the reconstruction quality in time domain. To this end, we compute the PCC of x_i with x_o .

Table 4 presents the mean and median values of ρ (x100) and F_Δ that were computed over the test set for each combination of domain and model. We can see that the same trend exists in all of domains – spectrogram based CNNs performs the best ordered by their depth. ConvE2E outperforms the HC3 and HC models (their performance is also ordered by depth). FC models perform the

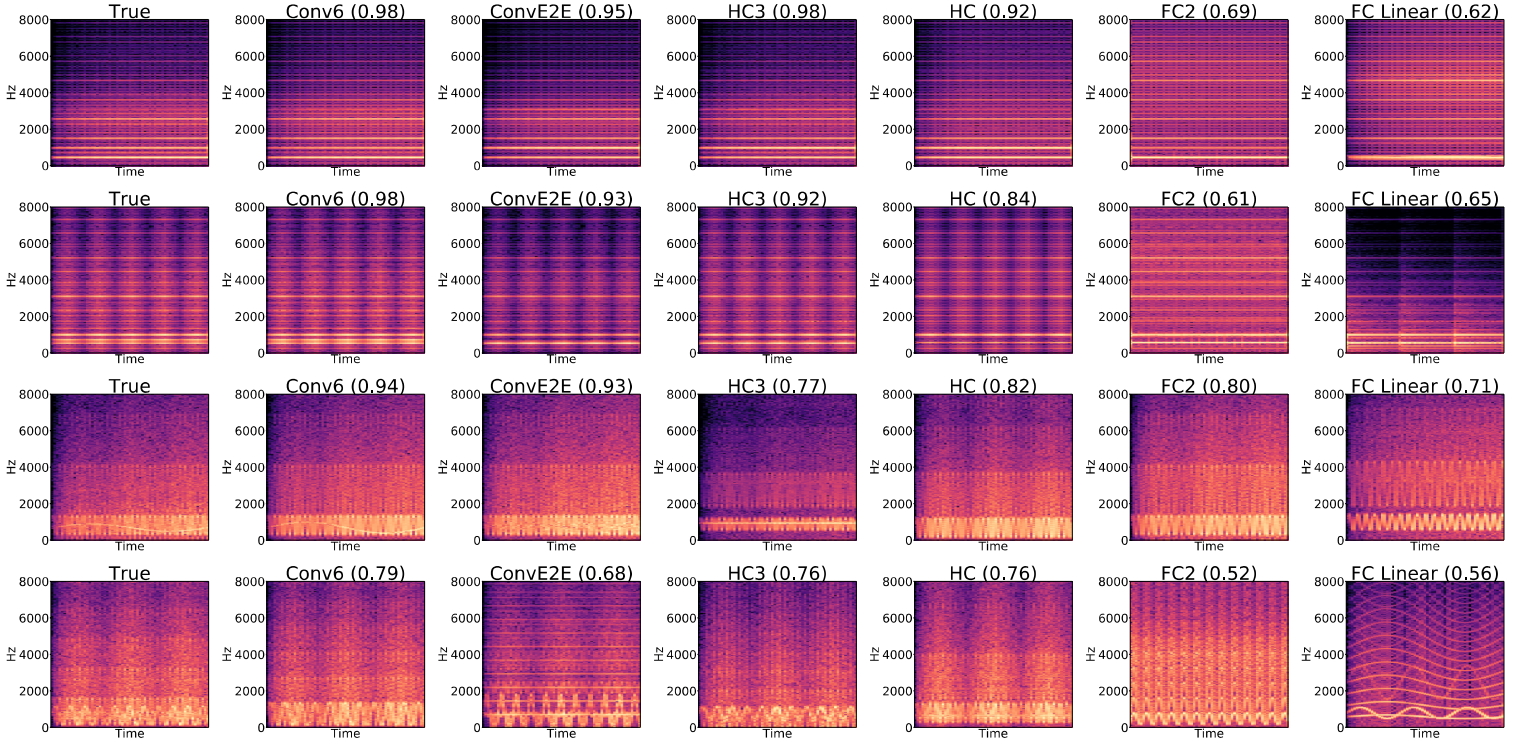


Figure 6. Four examples of spectrograms and their reconstructions, obtained by the evaluated models. See Section 6.2 for details

worst. Hence, we conclude that network depth contributes to the reconstruction quality as well. We further observe that PCC values obtained in time domain are significantly worse than PCC values obtained in frequency domain. This might be explained by the fact that the models are supplied with the STFT spectrogram in which the phase information is lost. Hence, we believe that if the phase information is fed to the models, an improvement in time domain PCC values is expected.

6.2 Qualitative Results

In this section, we present several examples that demonstrate the effectiveness of our method. These examples are not cherry picked and were randomly selected from the test set. The audio files of the examples are available online for the reader [15].

Figure 6 presents four examples. Each row corresponds to a different example and contains (left to right): the true spectrogram of the signal and the spectrograms obtained for the reconstructed signals using Conv6, ConvE2E, HC3, HC, FC2 and FC Linear models. In addition, for each reconstruction, we report the PCC value in the STFT domain. In what follows, we discuss each example (top to bottom).

The first example is of a signal with no frequency modulation and a mild amount of gating effect. We can see that the CNN and HC models produce parameter configurations that results in high quality reconstruction (both visually and in terms of PCC values). This is in contrast to the FC models that produce poor results: both reconstructions contain emphasized frequency bands that do not exist in the original signal. Moreover, the FC Linear model misses a dominating low frequency band that exists in the original signal.

The second example is of a signal with no frequency modulation, but with a decent amount of gating effect. In this example, Conv6 produces a nearly perfect reconstruction, while ConvE2E misses some of the low frequency bands and exhibits an attenuated

reconstruction. HC models seem to miss the same low frequency bands but exhibit less attenuation in high frequency bands. The FC2 model completely fails to recognize the gating effect and produces a reconstruction with emphasized frequency bands that do not exist in the original signal. The FC Linear model produces a wrong gating pattern and a severe attenuation of high frequency bands w.r.t the original signal.

The third example is of a frequency modulated signal with no gating. We can see that both Conv6 and ConvE2E produce decent reconstructions, while ConvE2E misses some of the FM pattern. HC3 produces a clearly worse reconstruction than HC and FC2, while FC linear ends up as the worst.

The last example is of a frequency modulated signal with a mild gating effect. We can see that Conv6 obtains a reconstruction that is the closest to the original spectrogram (visually), followed by the HCs models, while ConvE2E and FC models completely fail.

This limited set of examples demonstrates that spectrogram based CNNs of a sufficient depth outperform all other types of models across all scenarios. As part of our future research, we plan to conduct a human evaluation over a large set of examples in order to better understand the performance gaps between ConvE2E and the HC models, qualitatively.

7. CONCLUSION

In this paper, we proposed a method for automatic synthesizer parameter estimation from a source sound. The method is based on two models: spectrogram based CNN and an end-to-end CNN that are trained to predict the synthesizer parameter configuration from the STFT spectrogram and the raw audio, respectively. We demonstrate the effectiveness of the proposed method in a series of experiments and show that spectrogram based CNN outperform its end-to-end and HC counterparts, while both significantly outperform FC models.

8. REFERENCES

- [1] M. Russ, *Sound Synthesis and Sampling*. 2009.
- [2] E. J. Humphrey, J. P. Bello, and Y. LeCun, “Moving Beyond Feature Design: Deep Architectures and Automatic Feature Learning in Music Informatics,” *International Society for Music Information Retrieval Conference (ISMIR)*, no. Ismir, pp. 403–408, 2012.
- [3] E. J. Humphrey, J. P. Bello, and Y. Lecun, “Feature learning and deep architectures: New directions for music informatics,” *Journal of Intelligent Information Systems*, vol. 41, no. 3, pp. 461–481, 2013.
- [4] S. Dieleman and B. Schrauwen, “End-to-end learning for music audio,” in *ICASSP, IEEE International Conference on Acoustics, Speech and Signal Processing - Proceedings*, 2014, pp. 6964–6968.
- [5] K. Choi, G. Fazekas, and M. Sandler, “Automatic tagging using deep convolutional neural networks,” *International Society for Music Information Retrieval Conference*, pp. 805–811, 2016.
- [6] A. Goodfellow, Ian, Bengio, Yoshua, Courville, “Deep Learning,” *MIT Press*, 2016.
- [7] J. Riionheimo and V. Välimäki, “Parameter estimation of a plucked string synthesis model using a genetic algorithm with perceptual fitness calculation,” *Eurasip Journal on Applied Signal Processing*, vol. 2003, no. 8, pp. 791–805, 2003.
- [8] A. W. Y. Su and S. F. Liang, “A class of physical modeling recurrent networks for analysis/synthesis of plucked string instruments,” *IEEE Transactions on Neural Networks*, vol. 13, no. 5, pp. 1137–1148, 2002.
- [9] M. Sterling and M. Bocko, “Empirical physical modeling for bowed string instruments,” in *ICASSP, IEEE International Conference on Acoustics, Speech and Signal Processing - Proceedings*, 2010, pp. 433–436.
- [10] K. Itoyama and H. G. Okuno, “Parameter Estimation of Virtual Musical Instrument Synthesizers,” in *Proceedings of ICMC*, 2014, pp. 95–101.
- [11] <http://www.softsynth.com/jsyn>
- [12] Van Den Oord Aaron and K. Kavukcuoglu, “WaveNet: A Generative Model for Raw Audio,” *arXiv preprint arXiv:160903499*, 2016.
- [13] C. M. Bishop, *Pattern Recognition and Machine Learning*, vol. 4, no. 4. 2006.
- [14] D. P. Kingma and J. L. Ba, “Adam: a Method for Stochastic Optimization,” *International Conference on Learning Representations 2015*, pp. 1–15, 2015.
- [15] <https://github.com/deepsynth/deepsynth>
- [16] A. Krizhevsky, I. Sutskever, and G. E. Hinton, “ImageNet Classification with Deep Convolutional Neural Networks,” in *Advances in Neural Information Processing Systems 25*, 2012, pp. 1097–1105.
- [17] A. Graves, A. Mohamed, and G. E. Hinton, “Speech recognition with deep recurrent neural networks,” in *{IEEE} International Conference on Acoustics, Speech and Signal Processing, {ICASSP} 2013, Vancouver, BC, Canada, May 26-31, 2013*, 2013, pp. 6645–6649.
- [18] Y. Bengio, R. Ducharme, P. Vincent, and C. Janvin, “A Neural Probabilistic Language Model,” *J. Mach. Learn. Res.*, vol. 3, pp. 1137–1155, Mar. 2003.
- [19] W. Yih, K. Toutanova, J. C. Platt, and C. Meek, “Learning Discriminative Projections for Text Similarity Measures,” in *Proceedings of the Fifteenth Conference on Computational Natural Language Learning*, 2011, pp. 247–256.
- [20] T. Mikolov, I. Sutskever, K. Chen, G. S. Corrado, and J. Dean, “Distributed Representations of Words and Phrases and their Compositionality,” in *Advances in Neural Information Processing Systems 26*, 2013.
- [21] R. Collobert, J. Weston, L. Bottou, M. Karlen, K. Kavukcuoglu, and P. Kuksa, “Natural Language Processing (Almost) from Scratch,” *J. Mach. Learn. Res.*, vol. 12, pp. 2493–2537, Nov. 2011.
- [22] Y. Kim, “Convolutional Neural Networks for Sentence Classification,” *Proc. 2014 Conf. Empir. Methods Nat. Lang. Process. (EMNLP 2014)*, pp. 1746–1751, 2014.
- [23] Barkan, O. Bayesian Neural Word Embedding. AAAI 2017.